NANO LETTERS

2008
Vol. 8, No. 1
246−252

Normal and Shear Forces Generated during the Ordering (Directed Assembly) of Confined Straight and Curved Nanowires

Younjin Min,[†] Mustafa Akbulut,[§] Nataly Belman,[‡] Yuval Golan,[‡] Joe Zasadzinski,[†] and Jacob Israelachvili*,[†]

Department of Chemical Engineering, University of California, Santa Barbara, Santa Barbara, California 93106, Department of Chemical Engineering, Princeton University, A-306 Engineering Quadrangle, New Jersey 08544-5263, and Department of Materials Engineering, Ilse Katz Institute of Nanotechnology, Ben-Gurion University of the Negev, Beer-Sheva 84105, Israel

Received October 4, 2007; Revised Manuscript Received November 20, 2007

ABSTRACT

The effects of shape on nanowire interactions and shear-induced ordering were studied. Both the normal and lateral forces were sensitive to the particles' curvature. (i) No adhesion was observed between the confining surfaces, and the force profiles were short-ranged and mostly reversible for straight wires but longer-ranged and irreversible for curved wires. (ii) Structural phase transitions can occur in confined nanoparticle films. (iii) During shearing, straight wires order or align more easily than curved wires.

The unique and tunable properties of nanoparticle films make them suitable for applications such as quantum dot displays,[1−3] electronic devices,[4−6] photonic devices,[7−10] chemical and pressure sensors,[11−14] adhesion and friction modifiers,[15,16] lithographic application,[17,18] and high surface area to volume ratio catalysts.[19,20] It is known that the structure and properties of such films strongly depend on the processing method used and, of course, on the physical and chemical properties of the nanoparticles themselves including their size and shape. It is therefore important to understand the various forces and interactions acting between nanoparticles and the effects of confinement to better control their ordering into larger scale nanostructured materials.

The physical (mechanical and opto-electronic) and chemical properties of nanoparticles are often very different from those of the bulk materials, displaying some unique properties that depend on their size, shape, rigidity, internal composition, and surface functional groups. With the rapid development of new synthesis routes, one can produce nanoparticles of almost any composition and structure, each having different physical or chemical properties.

In the area of tribology, lubricating oils have traditionally contained ∼5 nm diameter surfactant-coated metal carbonate nanoparticle additives that are used more as antioxidants than for enhancing lubrication performance. The purely tribological benefits of using nanoparticles having different physical (rather than chemical) properties have only recently been investigated.[15,16,21] The tribological behavior of dry (i.e., water-free) nanoparticle lubricants or hydrocarbon lubricants containing colloidal or nanoparticle additives depends on the properties of the particles under confinement, such as the interparticle forces, their stiffness, yield strength (ability to resist delamination or material transfer), size, shape, polydispersity, and of course the nature of the confining surfaces and the loading and sliding conditions. For example, tribological forces are different from bulk viscous, viscoelastic, or rheological forces typically measured with rheometers, and under "tribological" conditions nanoparticles generally reorder differently from their ordering when sheared in the bulk. An additional feature that is important for any lubricant system is the ability to protect surfaces from damage or wear.

Clearly, there are many variables in any tribological system. Here, we focus on understanding the role of curvature on the normal and lateral forces of confined nanowires, which is both of fundamental interest and practical importance for (i) developing new micro- and nanoscale lubricant systems (nanorods were recently shown to be potentially better lubricant additives than spherical nanoparticles[22]) and (ii)

* Corresponding author. E-mail: jacob@engineering.ucsb.edu.
[†] University of California, Santa Barbara.
[§] Princeton University.
[‡] Ben-Gurion University of the Negev.

10.1021/nl072553e CCC: $40.75
Published on Web 12/11/2007

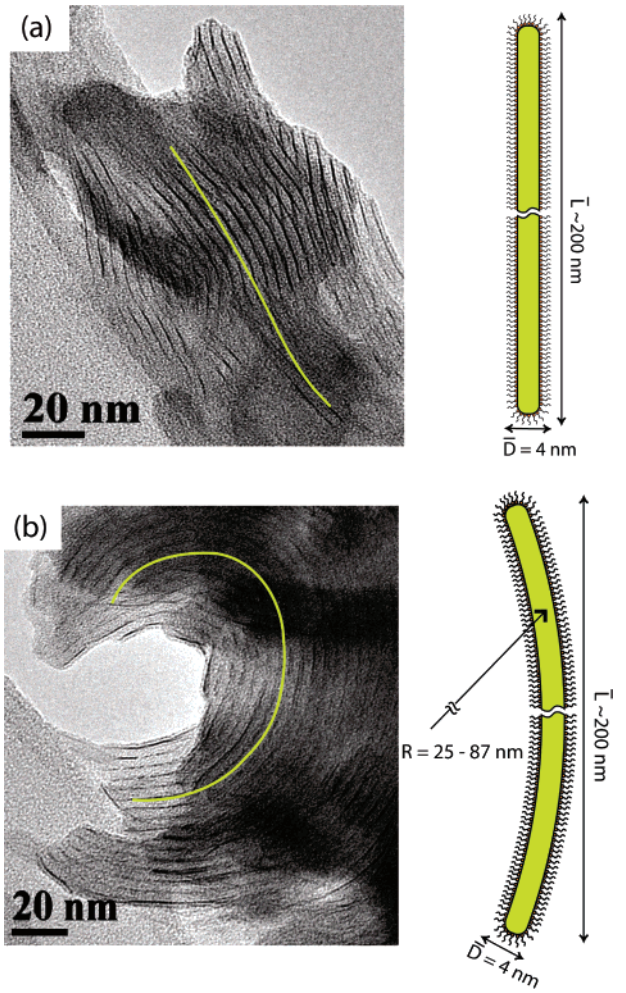

Figure 1. TEM images of (a) straight and (b) curved surfactant-coated ZnS−ODA nanowires with schematic drawings on the right. $\bar{L}$ is the mean length and $\bar{D}$ the width (diameter) of the wires studied. R is the radius of curvature of the curved nanowires. The TEM images were produced by depositing the nanowires from chloroform onto a holey carbon-coated TEM grid, drying, and imaging using a Tecnai G2 TEM operating at 120 kV. Under the experimental conditions, the nanowires were well dispersed in water-free dodecane, as previously proven by light scattering (see Figure 11 in ref 37); Figure 6b,i also shows the initial adsorbed condition of the nanowires before confinement.

understanding and controlling the processing of nonspherical nanoparticles into ordered nanostructured films and materials.

Straight and curved ZnS nanowires were synthesized using the method of Pradhan et al.[23,24] Zinc-ethylxanthate was dissolved in molten octadecylamine (ODA, $C_{18}H_{39}N$). The ODA-coated ZnS particles were harvested by flocculating the sample with methanol, centrifuging, and redispersing in chloroform. Potassium salt of ethylxanthic acid, zinc perchlorate hexahydrate (used for zinc-ethylxanthate preparation), and ODA (97% pure) were purchased from Aldrich and used as received. All nanoparticles had an outer diameter of ~4 nm, which consisted of a ~1.0 ± 0.1 nm ZnS core surrounded by a ~1.5 nm thick surfactant monolayer. The shapes of the nanoparticles are shown in the transmission electron microscopy (TEM) images in Figure 1. The lengths varied from 30 to 150 nm for the straight wires and 40−200 nm for the curved wires. The radii of the curved wires were 25−90 nm. We note that the straight wires were not perfectly straight along their full lengths.

A surface forces apparatus (SFA) was used to measure the normal forces between two initially curved molecularly smooth mica surfaces in dodecane containing 1 mg/mL of nanoparticles. The back surfaces of the 1−3 μm thick mica sheets were coated with a ~50 nm thick semi-reflecting layer of silver, required to obtain the optical interference "fringes of equal chromatic order" (FECO), which were used to record the following parameters, simultaneously and in situ: the surface separation, the shapes and deformations of the surfaces (and hence the uniformity of the trapped nanoparticle films), the flattened contact area, and the mean refractive index of the confined films.[25,26]

Normal forces $F_\perp$ were measured from the deflection of a horizontal double-cantilever spring supporting the lower surface. Two spring stiffnesses were used: $K = 1140$ and 11 000 N/m (stiffer springs allow for higher forces to be measured but at reduced sensitivity). Lateral motion was initiated by voltage-driven bimorph strips supporting the lower surface,[27] and the friction forces $F_{||}$ were measured using a vertical double-cantilever spring supporting the upper surface. These springs had resistance strain gauges attached to them for measuring the lateral deflection electronically, and hence the friction force between the two surfaces.

The nanoparticles were dispersed in dodecane in a glove box that was purged with dry nitrogen gas. Typical nanoparticle concentrations were ~1 mg/mL. Molecular sieves (8−12 mesh) were then added to the solutions to absorb any residual water. For the SFA experiments, a droplet of the appropriate dispersion was injected between two closely apposed mica surfaces, and the SFA chamber was sealed in an atmosphere of dry nitrogen gas together with a small Petri dish of P_2O_5 powder to ensure complete dryness during the experiments.

Figures 2 and 3 show the normal forces measured between two mica surfaces across straight and curved nanowire dispersions in dodecane. Figure 2 shows the weak, long-range forces, and Figure 3 shows the stronger, shorter-ranged forces. No attractive (adhesion) forces were measured either on approach (loading, compression) or separation (unloading, decompression). The forces were purely repulsive, revealing the essentially "steric" repulsion between the confined nanowires that had adsorbed (probably randomly) on each surface, analogous to the steric repulsion between polymer-coated surfaces. The measured force−distance curves were mostly reversible and reproducible for the same experimental conditions, for example, the same number of compression cycles, similar contact histories, etc., indicating that during compression few if any particles are squeezed out from between the surfaces into the surrounding solution reservoir.

Figure 2 shows some of the fine details of the long-range forces arising from the initial contact of the outermost ends of the wires on each surface. The curved wires gave rise to a longer-ranged repulsion (about twice the range), which was also very smooth and monotonic. The straight wires exhibited stepped discontinuities suggesting greater ordering within and/or between these layers or bundles as they rearranged.[28−30]

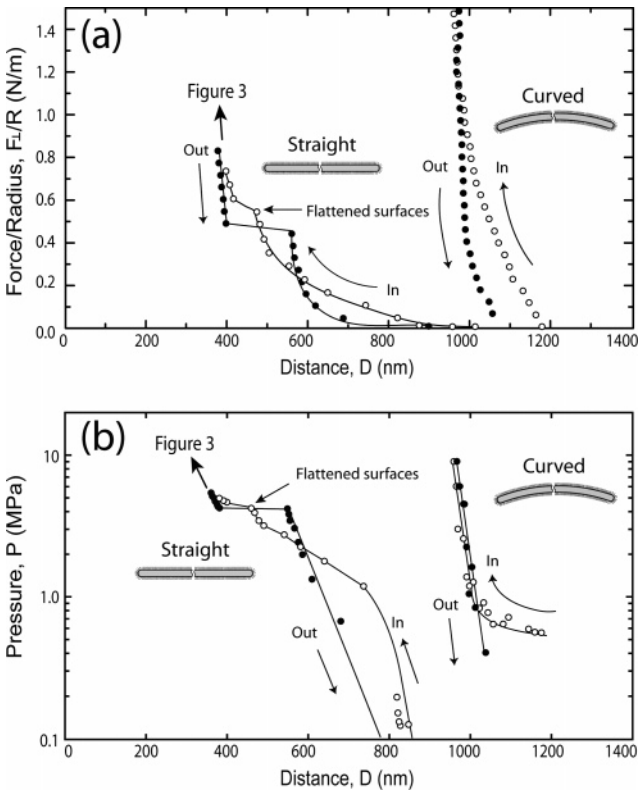

Figure 2. The weak, long range normal forces (a) and pressures (b) measured between two mica surfaces in a fully dried (dehydrated) solution of dodecane containing straight and curved 1 mg/mL ZnS−ODA nanowires. These forces were measured with the weak "normal force-measuring spring" of stiffness 1140 N/m. The radius R is the value for the undeformed surfaces. The points at which the surfaces started to noticeably flatten are indicted by arrows and the words "flattened surfaces". The kinks in the distance regime between 420 ± 20 and 460 ± 15 nm and F/R between 0.52 ± 0.01 and 0.57 ± 0.02 were reproducibly observed in four separate experiments.

Both of these effects are likely to be related to the higher reversibility in the forces across the curved wires compared to the straight wires. Also, the curved surfaces did not deform elastically (flatten) as they were pressed together across the curved wires, while across the straight wires elastic flattening occurred at pressures above ∼4 MPa, as indicated by point "flattened surfaces" in Figure 2. This flattening is again indicative of the more ordered layering in the case of the straight wires, which is also manifested in the higher forces/pressures measured, as shown in Figure 3.

The pressure plots of Figure 2b (and 3b) were obtained using the Derjaguin Approximation

$$E(D) = F(D)/2\pi R \tag{1}$$

to obtain the interaction energy E(D) between two planar surfaces per unit area, and then differentiating to get the pressure

$$P(D) = -\mathrm{d}E(D)/\mathrm{d}D = -[\mathrm{d}F(D)/\mathrm{d}D]/2\pi R \tag{2}$$

Once the surfaces flatten, the pressure can be obtained more directly by dividing the measured force by the flattened contact area, which can be measured from the flattened regions of the FECO fringes.[31−33]

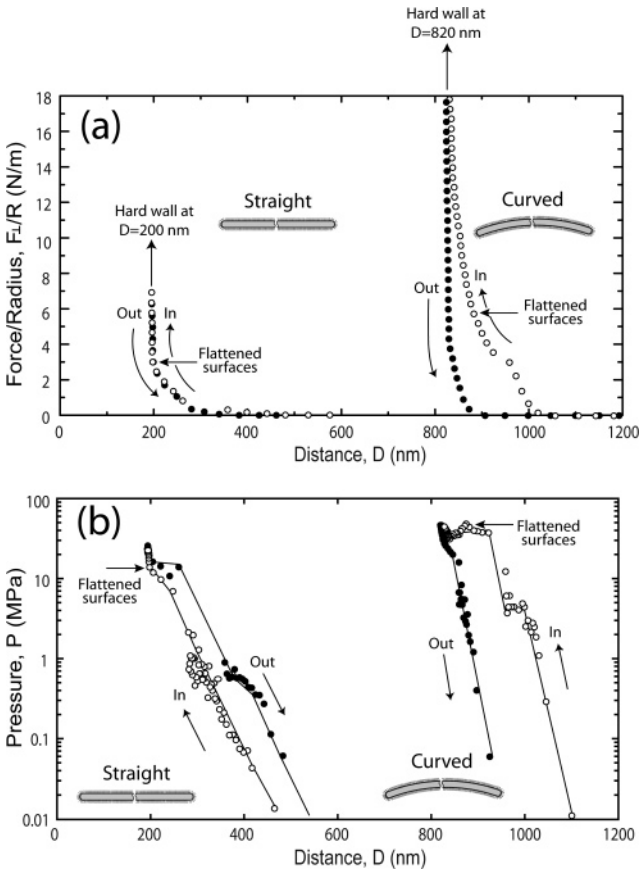

Figure 3. The stronger, short-range forces (a) and pressures (b) measured between two mica surfaces across straight and curved nanowires as in Figure 2 using a spring stiffness of 11 000 N/m. The points at which the surfaces started to noticeably flatten are indicted by arrows and the words "flattened surfaces". The drawn curves and lines are guides to the eye.

Figure 3 shows the forces measured with the stiffer spring, allowing for measurements to be made (on different samples) up to compressive forces and pressures of ∼50 MPa, which are more than an order of magnitude higher than with the weaker spring of Figure 2. For both types of nanowires, similar trends in the force profiles are still observed, especially the longer range and greater smoothness of the forces across the curved wires, and the short-range but sharp "hard-wall" and early flattening of the surfaces across the straight wires. In this case, however, the curved wires showed greater hysteresis than the straight wires, probably because the straight wires undergo their reordering at large separations and then become well ordered, that is, fully stacked and therefore no longer deformable under these conditions, while the curved wires are more elastic at large separations, being locked in their entangled state, but are forced to eventually reorder at high-compressive pressures. The surfaces confining straight nanowires reached a steep hard-wall at a separation of ∼200 nm, corresponding to about 50 layers of nanowires ordered parallel to the two surfaces. For the curved nanowires, the hard-wall is about four times thicker.

Refractive index measurements of the hard-wall films yielded 2.0 ± 0.1 and 1.55 ± 0.05 for the straight and curved

nanowires, respectively. Because the refractive index of the surfactant-coated nanowires is $n \approx 1.76$ (assuming one third from the ZnS of refractive index $n = 2.4$ and two thirds from the ODA of $n = 1.45$ for chains below their chain-melting temperature), the volume fraction of the straight nanowires is ~1.0, which implies that they are closely packed within the confined films (close-packed cylinders have a volume fraction of 0.91), while the curved nanowires constitute only 0.38 ± 0.14 of the compressed films. This shows, as might be expected, (i) that the straight nanoparticles are much more densely packed than the curved ones, and (ii) that on compression the nanowires can undergo significant orientational reordering.

Regarding the origins of the forces, the purely steric repulsion must come from (i) the elastic bending forces of the wires as they become compressed (these forces being reversible) and (ii) the rearrangements in local ordering (alignment, orientation) and plastic deformations of the wires, as manifested by the irreversibility or hysteresis in the loading−unloading force−distance curves[33] (although the organization and forces may eventually return to the original state in which case they may be described as "anelastic").

As noted above, reversible and irreversible behaviors appear to arise in different regions for the straight and curved nanowires, suggesting different regimes where major structural changes occur. Such structural changes can be identified more unambiguously by noting that eqs 1 and 2 allow us to identify regimes where structural phase transitions occur.[34,35] Thus, a linear region (one of constant slope) in the force versus distance or $F(D)$ plot, produces a horizontal line in the pressure versus distance or $P(D)$ plot between two planar surfaces. The latter is equivalent to a horizontal line in the pressure versus volume plot, which is the sign of a first-order phase transition and a coexistence region between the two turning points. In Figures 2 and 3, we notice such transitions for the straight and curved wires but at low pressures for the straight wires and at high pressures for the curved wires. These transitions need not be thermally driven but can also be athermal order−disorder or jamming−unjamming transitions of the Kirkwood−Alder type, as previously studied with large micron- to millimeter-sized colloidal particles.[35,36] For such transitions, the shapes and polydispersity of the particles are all-important, because they are determined entirely by the steric (repulsive hard-sphere or hard-particle) forces rather than the attractive forces.

Although this discussion has focused on the fine details and differences in the forces observed for these two systems when considered over many orders of magnitude, the forces are essentially (in a first approximation) exponentially repulsive, which has been observed before for confined nanoparticles and also for rough surfaces.[33,37−40] Further insights into these issues are obtained by comparing the normal forces with the lateral (shear) forces described below.

Figure 4 shows the initial and steady-state friction forces across the straight and curved nanowires under low and high loads. The forces were measured by cycling the surfaces back and forth over fixed shearing distances of 15−53 μm for the straight nanowires and 25−53 μm for the curved nanowires at fixed sliding velocities, V. Six panels are shown in all, each showing a typical "friction cycle" to illustrate the different features of the friction forces, including the initial or transient forces shown in the two left panels in Figure 4a,b. These transients are often different from the steady-state forces and provide information on how the

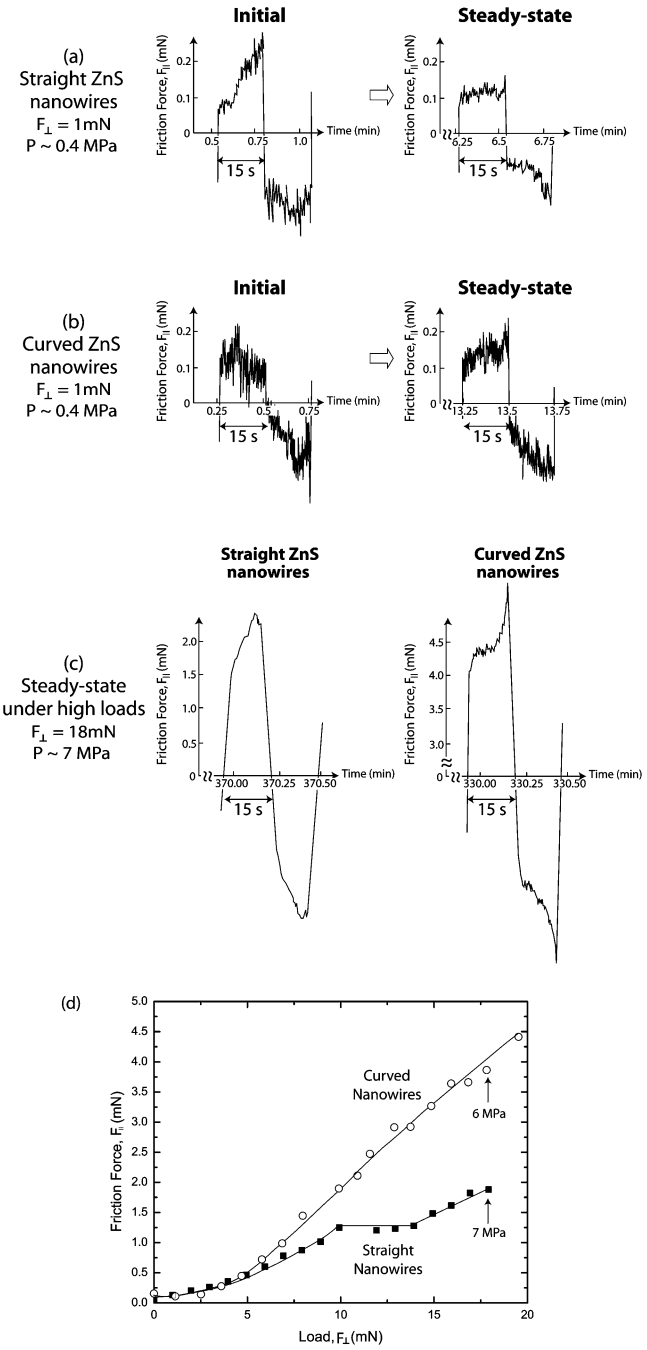

Figure 4. Friction force traces obtained during the back and forth shearing of two mica surfaces across films of (a) straight and (b) curved 1 mg/mL ZnS−ODA nanowires in dodecane over a distance of 30 μm (before reversing) and at a sliding velocity of 3.5 μm/s in both directions at low loads, and (c) both straight and curved nanowires at high loads. A typical cycle is shown in each case representing the initial (transient), and low- and high-load steady-state sliding. (d) Steady-state friction forces $F_{||}$ vs normal load $F_{\perp}$ for the two systems shown in (a−c).

particles adapt or reorganize themselves into the shearing configuration, which is generally accompanied by a concomitant change in the friction forces (and layer thickness) until steady-state conditions are achieved, as shown in the right panels in Figures 4a and 4b.

The following observations can be made: (i) Both systems display erratic variations in the initial "adaptation" regime of sliding, presumably reflecting the complex changes occurring in the gap. The initial regime lasted typically for 11 and 25 cycles for the straight nanowires and the curved nanowires, respectively, before steady-state conditions were achieved. (ii) At low loads and pressures, the steady-state friction forces are similar for both types of nanoparticles. However, at low loads, straight nanowires exhibit a considerable decrease in their friction force after the start of shearing, as shown in Figure 4a, whereas for curved nanowires there is no significant change in the friction force with time (Figure 4b). This suggests that the straight nanowires order or align during shearing, manifesting "shear thinning" behavior, and that they do this better than the curved wires. In addition, curved nanowires have more spikes in their friction traces than straight wires (cf. Figure 4a,b). (iii) At high loads (Figure 4c), the curved wires had about double the friction force as the straight wires, and steady-state conditions were attained within 5 cycles for both types of wires, that is, significantly faster or requiring a smaller shearing distance than at low loads.

Figure 4d shows the steady-state friction forces $F_{||}$ versus normal load $F_{\perp}$ at the same sliding speed of $V = 3.5\ \mu$m/s for both systems. The differences mentioned above are more clearly seen in this figure, especially the higher friction forces for the curved nanowires at higher loads. At low loads, the friction forces are very similar with both systems exhibiting low-friction coefficients of $\sim$0.025 which, increase to 0.10−0.25 at pressures above 10 MPa. Thus, even though for a given load the surface separation is significantly smaller for the straight nanowires, the curved nanowires show the higher friction forces. This is mainly due to their curved shapes and, therefore, increased entanglements during confinement and shear. The refractive index measurements, described earlier, also show that the curved wires are less densely packed and therefore more randomly ordered in different directions between the two surfaces during shearing.

Of particular interest in Figure 4d is the unchanging friction force starting at a load of $F_{\perp} \approx 10$ mN for the straight wires. This load coincides with the onset of the "structural transition" observed in the normal force measurements shown in Figure 2 at $F_{\perp}/R = 0.5$ N/m, which for $R = 2$ cm $= 0.02$ m occurred at a load of $F_{\perp} = 0.01$ N or 10 mN. To the best of our knowledge this observation is the first that shows a clear correlation between the normal and lateral (shear, friction) forces at a first-order phase transition. It suggests that in the two-phase coexistence regime where the normal pressure is not changing, the friction forces do not change either, which seems to be a very reasonable, almost self-evident, explanation.

Structural characterization and imaging of the nanowires were conducted as shown in Figures 5 and 6. Figure 5 shows

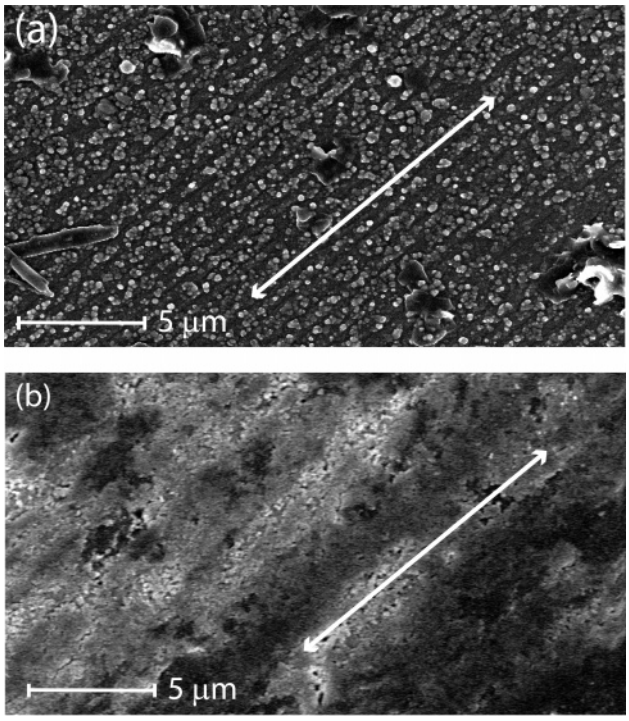

Figure 5. SEM images of the surfaces after shearing across (a) straight and (b) curved ZnS−ODA nanowires. The images were taken at the end of a shearing experiment after fully drying the surfaces.

scanning electron microscopy (SEM) images of the surfaces after shearing across the (a) straight and (b) curved ZnS−ODA nanowires. The surfaces were completely dried under nitrogen gas before they were imaged. We note that the straight nanowires exhibit a hierarchy of ordered structures and alignment along the shearing direction, while the curved wires appear to be almost random although some organization in the shearing direction is evident. Interestingly, neither structures appear to have ordered homogeneously, for example, with all the wires aligned in the same direction, as in a nematic liquid crystal. The striations observed with the straight nanowires are reminiscent of the shear bands observed when linear alkane molecules are sheared in molecularly thin films.[41] The way these striations were obtained here may provide a promising new approach to develop spatially ordered nanostructures via engineered assembly processes, which can be applicable to a wide variety of industrial purposes such as microelectronics, molecular recognition, chemical sensing, high-density data storage, and photonic devices.[42,43]

Figure 6a shows atomic force microscopy (AFM) images of the ZnS−ODA nanowires adsorbed on mica at different locations outside and between the two surfaces, as illustrated in Figure 6b. Outside the contact region (i), small uniform aggregates can be seen. Just within the contact junction (ii) where the confinement pressure was low, the structures have been compacted into large grains, and further inside the contact (iii) where the pressure was the highest these grains have become uniformly flattened into even larger grains. These images support the above suggestion that nanoparticle-based nanostructured thin films can be produced by confine-

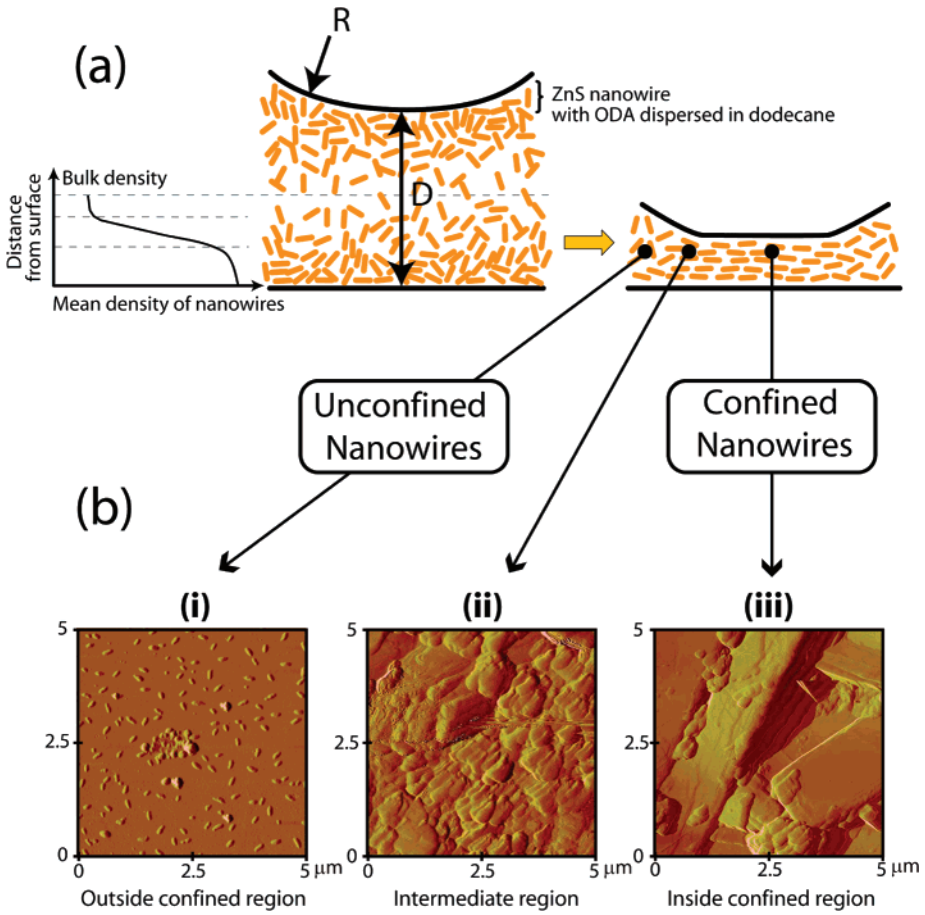

Figure 6. (a) AFM images of the straight ZnS−ODA nanowires adsorbed on mica at different regions of the two surfaces, as illustrated in (b). The images were taken after a loading experiment after drying the surfaces. (b) Schematic illustration of likely states of straight ZnS−ODA nanowires before and after confinement. Initially each surface has a diffuse, weakly adsorbed layer of nanoparticles on it. During compression the particles are compacted into a dense layer with a hard-wall surface. Curved wires achieve a lower density (about 4× lower judging by the 4× thicker hard-wall).

ment, and that their morphology can be further fine-tuned by applying normal pressure (and shear).

In summary, both straight and curved ZnS−ODA nanowires are found to have no mutual adhesion and exhibit exponential repulsion at all distances. However, we show that there is a strong effect of shape (such as nanowire curvature) on both the normal and lateral forces. The normal force curves of straight ZnS−ODA nanowires suggest jamming transitions, implying rearrangement of the nanowires to an ordered state at certain distances in agreement with the friction results. The curved nanoparticles have a longer-ranged steric repulsion and a thicker hard-wall layer than straight nanowires under compression. The "history" of previous compression cycles also had a role in the force profiles; for example, the first force run was different from the rest, and the following consecutive force profiles showed similar magnitudes and ranges of the forces. We further show that the straight nanowires can be ordered better and easier than curved ones, but with a certain critical pressure of $P \sim 2$ MPa being required for ordering under confinement (Figure 4d). Straight ZnS−ODA nanowires show significantly reduced friction force values suggesting their greater effectiveness as lubricant additives.

Fundamentally, our results obtained clearly point out that these nanoparticles can constitute an intermediate regime between "close-to-equilibrium" atomic and molecular fluids and macroscopic-scale "far-from-equilibrium" systems and interactions. It should be noted that ordered nanostructures (engineered assemblies) newly produced during both compressing and shearing processes are totally different from thermodynamically organized ones (self-assemblies) and can be more useful in a practical point of view. We demonstrate that these assemblies can be obtained by varying external factors such as the normal and lateral forces mainly depending on the induced confinement.

This study also provides practical scientific and technical insights into how nanoparticles can be organized into well-defined films. Furthermore, we illustrate how such nanoparticles will behave either in the bulk or in confined geometries, which strongly depend on their curvature, suggesting that controlling the shape of nanoparticles can be one excellent starting point for the manipulation of their assemblies. The engineered assembly process described here provides a versatile route to create spatially arranged nanostructures, which have many potential applications for optoelectronic devices, catalysis, chemical and biological sensing, and high-density data storage.

Acknowledgment. Y.G. and J.I. thank the U.S.−Israel Binational Science Foundation, Grant 2006032, M.A. thanks

the ONR under Grant N00014-05-1-5040, and Y.M. thanks the MRSEC Program of the NSF under Award Number DMR05-20415 for substantially supporting this work.

References

(1) Alivisatos, A. P. *Science* **1996**, *271* (5251), 933−937.
(2) Chan, W. C. W.; Nie, S. M. *Science* **1998**, *281* (5385), 2016−2018.
(3) Dubertret, B.; Skourides, P.; Norris, D. J.; Noireaux, V.; Brivanlou, A. H.; Libchaber, A. *Science* **2002**, *298* (5599), 1759−1762.
(4) Huang, Y.; Duan, X. F.; Cui, Y.; Lauhon, L. J.; Kim, K. H.; Lieber, C. M. *Science* **2001**, *294* (5545), 1313−1317.
(5) Cui, Y.; Bjork, M. T.; Liddle, J. A.; Sonnichsen, C.; Boussert, B.; Alivisatos, A. P. *Nano Lett.* **2004**, *4* (6), 1093−1098.
(6) Duan, X. F.; Huang, Y.; Cui, Y.; Wang, J. F.; Lieber, C. M. *Nature* **2001**, *409* (6816), 66−69.
(7) Xia, D. Y.; Li, D.; Luo, Y.; Brueck, S. R. J. *Adv. Mater.* **2006**, *18* (7), 930−933.
(8) Vlasov, Y. A.; Bo, X. Z.; Sturm, J. C.; Norris, D. J. *Nature* **2001**, *414* (6861), 289−293.
(9) Rogach, A.; Susha, A.; Caruso, F.; Sukhorukov, G.; Kornowski, A.; Kershaw, S.; Mohwald, H.; Eychmuller, A.; Weller, H. *Adv. Mater.* **2000**, *12* (5), 333−337.
(10) Ozin, G. A.; Yang, S. M. *Adv. Funct. Mater.* **2001**, *11* (2), 95−104.
(11) Andersson, H.; van der Wijngaart, W.; Stemme, G. *Electrophoresis* **2001**, *22* (2), 249−257.
(12) Scott, R. W. J.; Yang, S. M.; Coombs, N.; Ozin, G. A.; Williams, D. E. *Adv. Funct. Mater.* **2003**, *13* (3), 225−231.
(13) Favier, F.; Walter, E. C.; Zach, M. P.; Benter, T.; Penner, R. M. *Science* **2001**, *293* (5538), 2227−2231.
(14) Tolbert, S.; Alivisatos, A. *Annu. Rev. Phys. Chem.* **1995**, *46*, 595−625.
(15) Rapoport, L.; Fleischer, N.; Tenne, R. *Adv. Mater.* **2003**, *15* (7−8), 651−655.
(16) Rapoport, L.; Bilik, Y.; Feldman, Y.; Homyonfer, M.; Cohen, S. R.; Tenne, R. *Nature* **1997**, *387* (6635), 791−793.
(17) Burmeister, F.; Schafle, C.; Matthes, T.; Bohmisch, M.; Boneberg, J.; Leiderer, P. *Langmuir* **1997**, *13* (11), 2983−2987.
(18) Ingert, D.; Pileni, M. P. *J. Phys. Chem. B* **2003**, *107* (36), 9617−9619.
(19) Al-Daous, M. A.; Stein, A. *Chem. Mater.* **2003**, *15* (13), 2638−2645.
(20) Velev, O. D.; Tessier, P. M.; Lenhoff, A. M.; Kaler, E. W. *Nature* **1999**, *401* (6753), 548−548.
(21) Katz, A.; Redlich, M.; Rapoport, L.; Wagner, H. D.; Tenne, R. *Tribol. Lett.* **2006**, *21* (2), 135−139.
(22) Akbulut, M.; Belman, N.; Golan, Y.; Israelachvili, J. *Adv. Mater.* **2006**, *18* (19), 2589−2592.
(23) Pradhan, N.; Katz, B.; Efrima, S. *J. Phys. Chem. B* **2003**, *107* (50), 13843−13854.
(24) Pradhan, N.; Efrima, S. *J. Phys. Chem. B* **2004**, *108* (32), 11964−11970.
(25) Israelachvili, J. N. *J. Colloid Interface Sci.* **1973**, *44* (2), 259−72.
(26) Heuberger, M.; Luengo, G.; Israelachvili, J. *Langmuir* **1997**, *13*, 3839−48.
(27) Luengo, G.; Schmitt, F. J.; Hill, R.; Israelachvili, J. *Macromolecules* **1997**, *30* (8), 2482−2494.
(28) Colton, R. J. *J. Vac. Sci. Technol., B* **2004**, *22* (4), 1609−1635.
(29) Klein, J.; Kumacheva, E. *Science* **1995**, *269* (5225), 816−819.
(30) Moreau, L.; Richetti, P.; Barois, P. *Phys. Rev. Lett.* **1994**, *73* (26), 3556−3559.
(31) Benz, M.; Gutsmann, T.; Chen, N. H.; Tadmor, R.; Israelachvili, J. *Biophys. J.* **2004**, *86* (2), 870−879.
(32) Horn, R. G.; Israelachvili, J. N.; Pribac, F. *J. Colloid Interface Sci.* **1987**, *115* (2), 480−492.
(33) Akbulut, M.; Alig, A. R. G.; Min, Y.; Belman, N.; Reynolds, M.; Golan, Y.; Israelachvili, J. *Langmuir* **2007**, *23* (7), 3961−3969.
(34) Israelachvili, J. *Intermolecular and Surface Forces*; Academic Press: San Diego, CA, 1991.
(35) Trappe, V.; Prasad, V.; Cipelletti, L.; Segre, P. N.; Weitz, D. A. *Nature* **2001**, *411* (6839), 772−775.
(36) Bourlinos, A. B.; Herrera, R.; Chalkias, N.; Jiang, D. D.; Zhang, Q.; Archer, L. A.; Giannelis, E. P. *Adv. Mater.* **2005**, *17* (2), 234−237.
(37) Alig, A. R. G.; Akbulut, M.; Golan, Y.; Israelachvili, J. *Adv. Funct. Mater.* **2006**, *16* (16), 2127−2134.
(38) Gourdon, D.; Yasa, M.; Alig, A. R. G.; Li, Y. L.; Safinya, C. R.; Israelachvili, J. N. *Adv. Funct. Mater.* **2004**, *14* (3), 238−242.
(39) Benz, M.; Rosenberg, K. J.; Kramer, E. J.; Israelachvili, J. N. *J. Phys. Chem. B* **2006**, *110* (24), 11884−11893.
(40) Rau, D. C.; Lee, B.; Parsegian, V. A. *Proc. Natl. Acad. Sci. U.S.A.* **1984**, *81* (9), 2621−2625.
(41) Drummond, C.; Israelachvili, J. *Macromolecules* **2000**, *33* (13), 4910−4920.
(42) Lin, Y.; Boker, A.; He, J. B.; Sill, K.; Xiang, H. Q.; Abetz, C.; Li, X. F.; Wang, J.; Emrick, T.; Long, S.; Wang, Q.; Balazs, A.; Russell, T. P. *Nature* **2005**, *434* (7029), 55−59.
(43) Gittins, D. I.; Susha, A. S.; Schoeler, B.; Caruso, F. *Adv. Mater.* **2002**, *14* (7), 508−512.

NL072553E